RANS COMPUTATIONS OF A CAVITATING TIP VORTEX

Jean, Decaix[1]
Address
Route du Rawyl 47, 1950 Sion, Switzerland
Mailing address
jean.decaix@hevs.ch
Phone: +41 27 606 88 25, Fax: +41 27 606 88 15

Guillaume, Balarac
Mailing address
guillaume.balarac@legi.grenoble-inp.fr

Cécile, Münch
Mailing address
cecile.muench@hevs.ch

KEY WORDS

k-ω SST model, Kunz model, NACA 0009, OpenFOAM

ABSTRACT

The Swiss national research project Hydronet 2 gathers a consortium of industrial and academic partners supported by the Competence Center of Energy and Mobility (CCEM) and Swiss Electric Research (SER) in order to improve the hydropower plants. One of the research topic focuses on the cavitating tip vortex. Such a vortex takes place in axial turbines as Kaplan turbines used for producing hydroelectricity. This phenomenon drives a lot of drawbacks such as erosion, unsteady flow rate and a decrease of the turbine efficiency. To better understand the behaviour of the tip vortex, computations of a simple test case are performed. The test case consists in a NACA profile mounted in a channel with a gap between the NACA tip and the lateral wall. The computations are carried out with the OpenFOAM solver both in one-phase and two-phase flow. The turbulent motion is modelled with a RANS approach. For the two-phase flows computations, the phase change between liquid and vapour is achieved with the model proposed by Kunz. The results will be compared in cavitating and non cavitating cases with the experimental data provided by the EPFL Laboratory for Hydraulic Machines. The comparisons deal with global picture of the flow, the trajectory of the tip vortex and the velocity field downstream the NACA profile.

1. INTRODUCTION

A tip vortex develops when an obstacle of finite span is immersed in a flow. Tip vortices can be encountered both in external and internal flows. External flows can be illustrated by the helicopter rotor blades or by aircraft wings, for which, the tip vortex develops at the end of the wing close to the leading edge. For the external tip vortices, the researches focus on the vortex growth and decrease. Internal flows that involve tip vortices are encountered in aircraft engines or hydraulic turbines. In these cases, the influence of the gap between the balde and the stator is of the most importance. A large part of the studies are confined to one-phase flows due to the difficulties to perform measurements and numerical simulations for two-phase flows.

For one-phase flow, several experimental studies investigate the influence of the gap width on the tip vortex behavior ([1],[2]). One of the most documented studies was performed by Devenport ([3],[4]) in the case of a compressor cascade. Overall, these studies focus on the field downstream the blade by analyzing the mean and turbulent flow and the influence of a moving end wall. The turbulent flow is not isotropic since the longitudinal fluctuations dominate. Moreover, the endwall motion does not affect the main features

[1] Corresponding author

of the tip vortex. An attention is also devoted to the wandering motion of the tip vortex. This phenomenon is not well understood, particularly, it is not clear if the wandering depends on the experimental tunnel [5].

Numerically, the tip vortex was investigated using various models as vortex methods [6], Reynolds Averaged Navier Sokes (RANS) approach coupling with an eddy-viscosity model [7] or second moment closure [8], or Large Eddy Simulation [9]. In [10], the author use the Joseph criterion to determine the regions that can be affected by cavitation. Nevertheless, no cavitation simulations has been attempted.

Since several years, cavitating flows has been experimentaly investigated in various configurations. Some studies focus on the tip vortex ([11],[12]). The study of Miorini gives information of the velocity field inside the gap due to PIV measurements. However, the measurements are rarely available inside the vortex. Regarding the computations, only few attempts has been performed ([13],[14]) using RANS or ILES (Implicit LES) modeling. The validations are often restricted to flow vizualisations.

The present work consists in the computation of a truncated Naca 0009 profile mounted in a channel. The computations are carried out with the OpenFOAM solver release 2.1.0. Previous RANS and LES computations without cavitation have been already performed [15]. In the present study, a non cavitating case is firstly computed and compared with experimental measurements provided by the Laboratory of Hydraulics Machines – Swiss Federal Institute of Technology Lausanne [16]. Then, cavitation is introduced in the simulation. Results are discussed by comparisons between the cavitating and non-cavitating cases.

2. FLOW MODELLING

The OpenFOAM solver provides various turbulence and cavitation models. For the present computations, the two-phase flow is modelled using a homogeneous relaxation model. Therefore, the two phases are considered to share the same velocity, the same temperature and the same pressure. The mixture density is computed as:

$$\rho = \alpha_L \rho_L + (1 - \alpha_L)\rho_V \tag{1}$$

With α_L, the liquid volume fraction and ρ_L and ρ_V, respectively the liquid and the vapour density.
The RANS equations for the mixture read:

$$\begin{gathered} \frac{\partial \rho}{\partial t} + \frac{\partial \rho \bar{u}_i}{\partial x_i} = 0 \\ \frac{\partial \rho \bar{u}_i}{\partial t} + \frac{\partial \rho \overline{u_j} \overline{u_i}}{\partial x_j} = -\frac{\partial \bar{p}}{\partial x_i} + \frac{\partial (\sigma_{ij} + \tau_{ij})}{\partial x_j} \end{gathered} \tag{2}$$

With σ_{ij} the viscous stresses and τ_{ij} the turbulent stresses defined as:

$$\begin{aligned} \sigma_{ij} &= \rho \nu \left(\frac{\partial \bar{u}_i}{\partial x_j} + \frac{\partial \bar{u}_j}{\partial x_i} \right) \\ \tau_{ij} &= -\rho \, \overline{u_i' u_j'} = \rho \nu_t \left(\frac{\partial \bar{u}_i}{\partial x_j} + \frac{\partial \bar{u}_j}{\partial x_i} \right) \end{aligned} \tag{3}$$

ν is the kinematic molecular viscosity and ν_t the kinematic turbulent eddy-viscosity. The overbar and the prime superscript denote respectively the mean and the turbulent parts.

The turbulent eddy-viscosity ν_t is computed using the *k-ω* SST model [17]:

$$\nu_t = \frac{a_1 k}{\max(a_1 \omega, S F_2)} \tag{4}$$

With *k* the turbulent kinetic energy, *ω* the turbulence frequency, S the invariant measure of the strain rate, F_2 a blending function and $a_1 = 0.31$.

The liquid volume fraction α_L is computed using a transport equation that reads:

$$\frac{\partial \alpha_L}{\partial t} + \bar{u}_j \frac{\partial \alpha_L}{\partial x_j} = m_v + m_c \tag{5}$$

m_v and m_c are respectively the vaporization and the condensation source term. These two terms are estimated using a derivation of the Kunz's model [18]:

$$m_v = \frac{\rho}{\rho_L}\frac{C_v}{t_\infty}\frac{\min(p-p_{vap},0)}{0.5\,\rho_L U_\infty^2}$$
$$m_c = \frac{\rho}{\rho_L}\frac{C_c}{t_\infty}\alpha_L^2\,\frac{\max(p-p_{vap},0)}{\max\left(p-p_{vap},0.01\,p_{vap}\right)} \quad (6)$$

With p_{vap} the vaporisation pressure, U_∞ a velocity reference, t_∞ a relaxation time and C_v and C_c two empirical parameters specified by the user.

3. TEST CASE

The test case consists in a Naca 0009 blade with a truncated trailing edge mounted in a channel. The chord blade length c is of 0.1 m, the angle of attack i is of 10 degrees and the gap width τ divided by the chord length is $\tau/c = 0.1$. The cross section is a square of length 1.5 c. The inlet velocity is set to $U_\infty = 10.2$ m/s.

The computational domain extends two chords upstream the leading edge and five chords downstream the trailing edge (**Figure 1**). The equations are discretised on a structured mesh containing approximately 2 millions of nodes. The gap region is filled with 30 nodes. The boundary conditions are:

- At the inlet: $u_x = 10.2$ m/s $u_y = u_z = 0$ m/s.
- At the outlet: a convective condition is applied. Pressure reference is provided at a point located *1.3 c* upstream the trailing edge.
- Walls: no slip condition with the use of an extended wall law.

The system of equations is solved using a mix of the SIMPLE and PISO algorithms called PIMPLE algorithm in the OpenFOAM framework. The time step is set to 10^{-5} s.

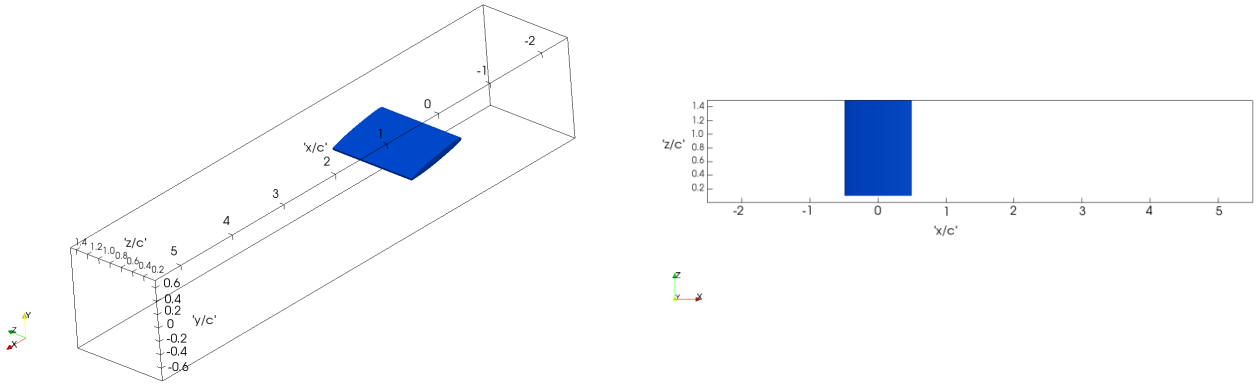

Figure 1: Computational domain: 3D view (left) and top view (right).

4. RESULTS

4.1 Computation without cavitation

Figure 2 displays the tip vortex identified using the Q-criterion and the three planes where the experimental data are available. To assess the accuracy of the computation, the centre of the vortex is determined using the maximum of the axial vorticity. **Table 1** gathers the position of the vortex both for the experiment and the computation. Overall, the discrepancy is lower than 15%, excepted for the *y*-position at *x/c = 0.15* m. **Figure 3** shows the contour of the velocity components. The axial velocity acceleration on the left side of the vortex is capture by the computation even if the magnitude is slightly under-estimated. The high magnitude of the crosswise components is also capture. It is noticeable that compared to the experiment, the computation diffuses the gradient of the crosswise components in the core of the vortex. Therefore, the value of the axial vorticity in the core of the vortex is underestimated. Nevertheless, focusing on the iso-contour of the axial vorticity near the vortex centre (**Figure 4**), the vorticity is well resolved since the iso-line matches. It can be concluded that the RANS computation is able to provide results in accordance with the experiment.

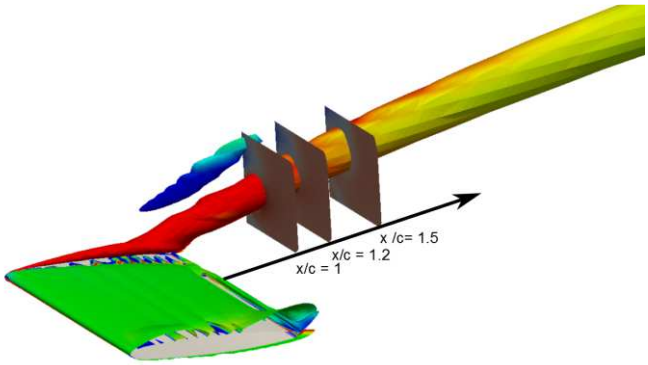

Figure 2: Tip vortex determined with the Q-criterion and location of the experimental measurement planes.

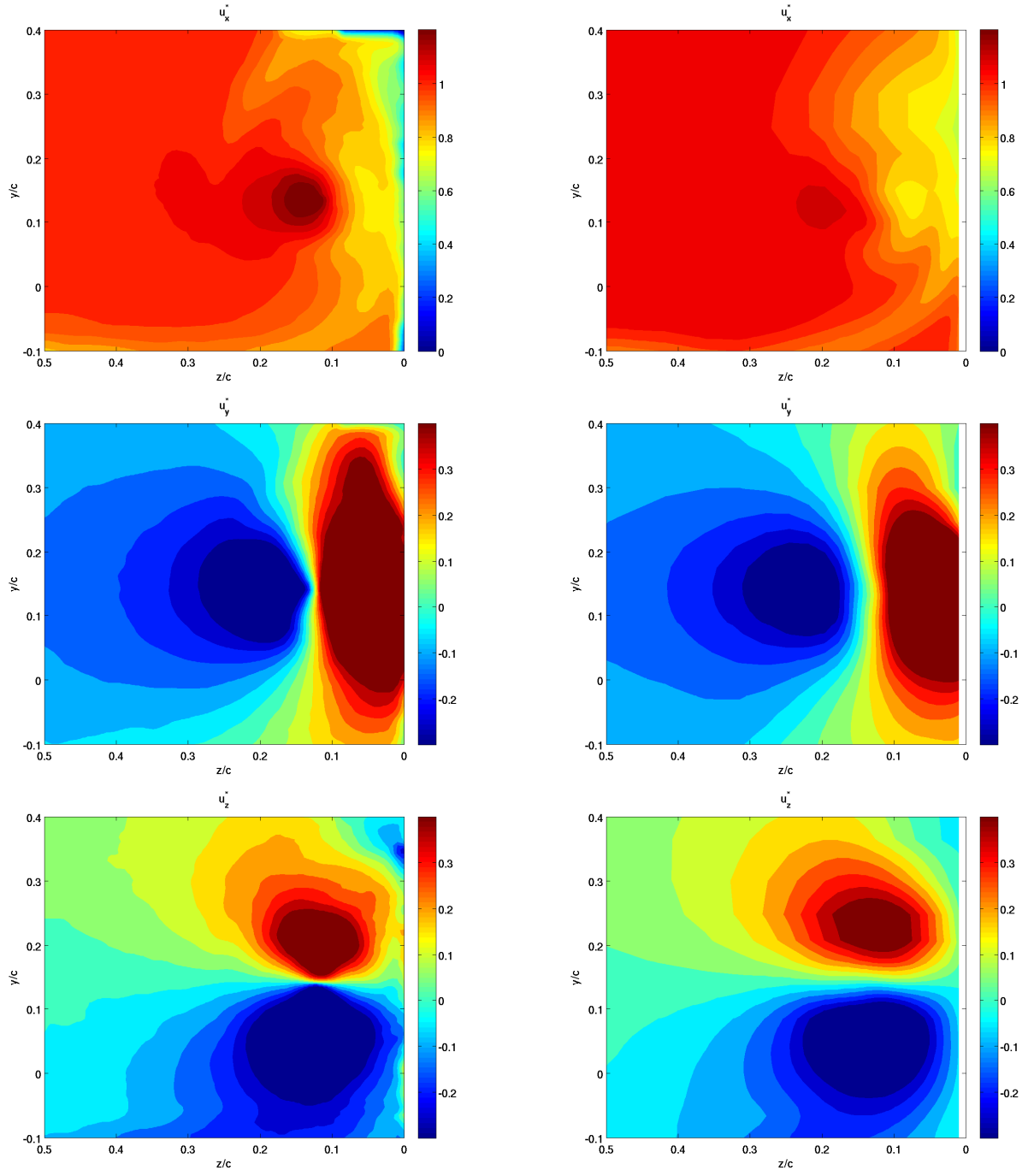

Figure 3: Contour of the velocity components (downstream view). Experiment (left) and RANS (right).

Table 1: Position of the centre of the tip vortex

x/c	y/c (Experiment)	y/c (RANS)	z/c (Experiment)	z/c (RANS)
1	0.14	0.13	0.12	0.1
1.2	0.18	0.18	0.13	0.12
1.5	0.3	0.22	0.16	0.15

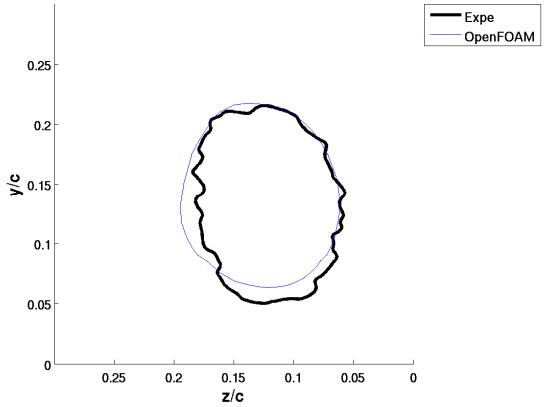

Figure 4: Iso-line of the non-dimensional axial vorticity ($\Omega_x^* = 10$ at $x/c = 1$).

4.2 Computation with cavitation

For the cavitating computation, the parameters of the cavitation model are set to:

- $t_\infty = 0.001$ s.
- $U_\infty = 10$ m/s.
- $p_{vap} = 255\,000$ Pa.
- $C_c = 500$ and $C_v = 3\,500$.

The value of p_{vap} can be explained by the fact that the vorticity inside the vortex core is under-estimated. Indeed, such an underestimation leads to an over-estimation of the pressure inside the vortex. Therefore, the expected low pressure inside the vortex (approximately $p_{vap} = 2\,330$ Pa at 293 K) cannot be reached. A first computation performed at the same cavitation parameter $\sigma_v = 2.1$ that the experiment was not able to provide a cavitating tip vortex. A second computation at $\sigma_v = 1.3$ provides a cavitating tip vortex that can be compared qualitatively with the experiment. The iso-contour of the liquid volume fraction (**Figure 5**) shows that cavitation appears mainly in the core of the vortex and in the gap. No cavitation is observed on the suction side, except a thin layer at the leading edge.

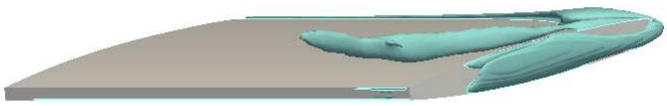

Figure 5: Iso-contour of the liquid volume fraction ($\alpha_L = 0.9$).

Experimental data are restricted to high speed viewings. **Figure 6** shows a superposition of an experimental view of the tip vortex and the iso-contour of the liquid volume fraction provided by the computation. The trajectory of the cavitating tip vortex is well predicted by the computation. The volume occupied by the tip vortex is slightly larger for the computation than the experiment.

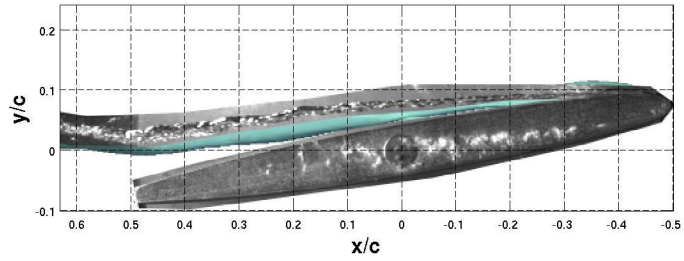

Figure 6: Superposition of the tip vortex between the experiment (in front) and the RANS computation (behind).

The results are also compared with the computation without cavitation. The mean axial velocity field is strongly affected by the presence of cavitation (**Figure 7**). Indeed, for the cavitating computation, the boundary layer separates on the suction side. This is caused by the presence of the thin film of cavitation at the leading edge. Moreover, the trajectory of the tip vortex downstream the trailing edge is modified. **Figure 8** represents the tip vortex trajectory projected on an x-y plane and an x-z plane. The *y*-position is lower with cavitation than without cavitation. The *z*-position is closer to the sidewall in case of cavitation. These two features can be explained by the separation of the flow on the suction side. The separation decreases the pressure difference between the pressure side and suction side leading to a lower *y* value and involves a larger wake, which prevents the tip vortex from moving to the centre of the channel.

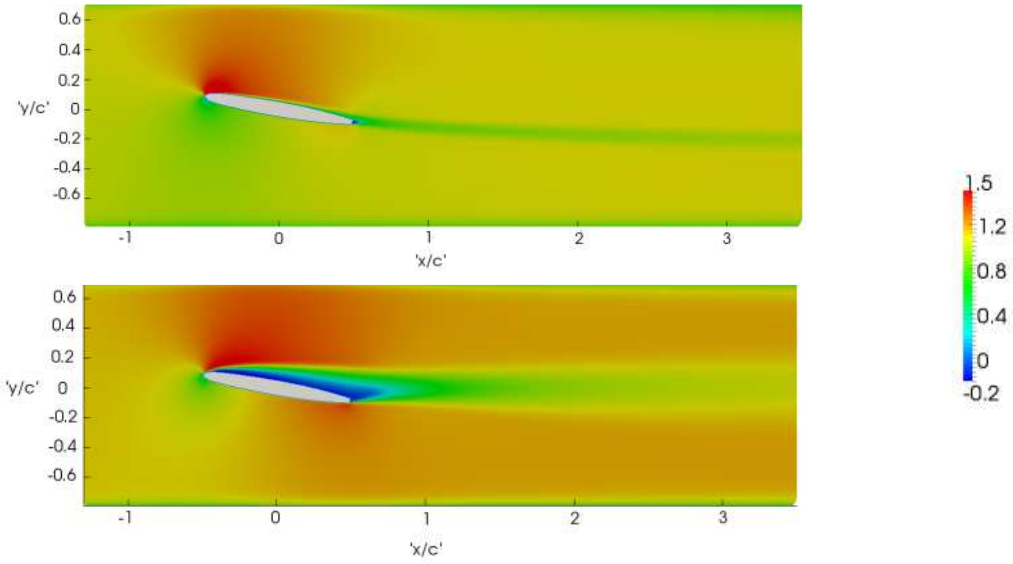

Figure 7: Mean axial velocity field in the mid span section. Computation without cavitation (top) and with cavitation (bottom).

5. CONCLUSION

Computations of the tip vortex including the gap between the blade and the side wall are performed for cavitating and non cavitating configurations. The non-cavitating computation is assessed compared with experimental data available downstream the trailing edge. Results based on the vortex trajectory and the velocity field show few discrepancies between the experiment and the computations. However, an inability of the computation to resolve the vorticity in the core of the vortex is put in evidence even if the vorticity near the vortex core is well capture. This feature prevents the computation from predicting an accurate drop in pressure in the vortex core. Consequently, the computation with cavitation cannot be carried out for the same operating point that experimentally. Adjusting the operating point, a cavitating tip vortex can be obtained with a qualitative agreement with the experiment. The computation put in evidence that the developement of cavitation involves a separation of the boundary layer on the suction side. Therefore, the

tip vortex trajectory downstream the trailing edge is modified. Particularly, the vortex evolves closer to the sidewall, which can enhance erosion problems.

The results make appear that additional works are needed. For instance, the development of methods that can allow resolving the vorticity inside the vortex core and performing cavitating computations at the same operating point than the experiment. Moreover, experimental data inside the cavitating vortex will be welcome in order to assess the relevance of the parameters used for the cavitation model.

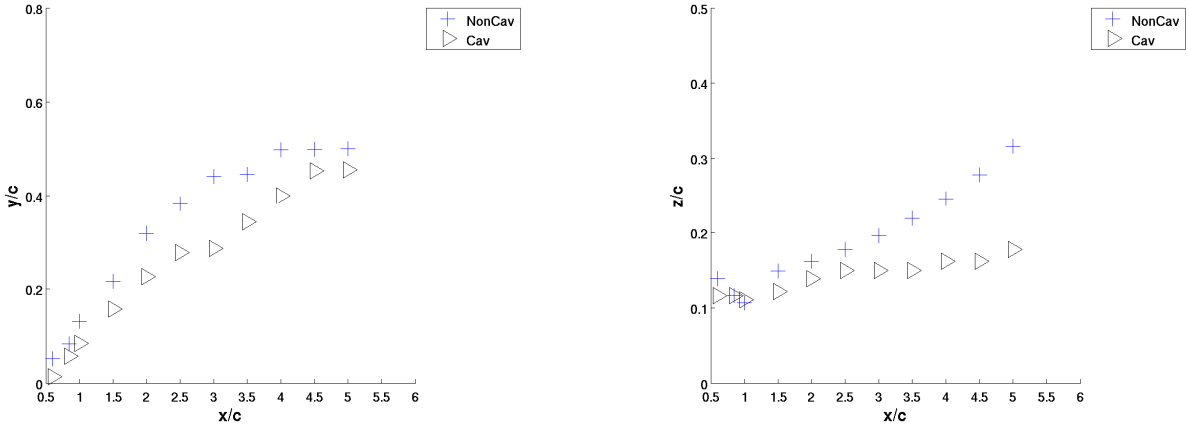

Figure 8: Position of the centre of the vortex projected in an x-y plane (left) and x-z plane (right).

NOMENCLATURE

α_L	Liquid volume fraction.
σ_v	Cavitation parameter.
c	Chord length (m).
i	Angle of incidence (degree).
k	Turbulent kinetic energy (m2/s2).
p	Pressure field (Pa).
p_{vap}	Vaporisation pressure (Pa)
u_i	Velocity field (m/s).
ν	Molecular kinematic viscosity (m2/s).
ν_t	Turbulent eddy-viscosity (m2/s).
ω	Turbulence frequency (1/s).
σ_{ij}	Viscous stress tensor (kg/(m.s2).
τ_{ij}	Reynolds stress tensor (kg/(m.s2).
τ	Gap width (m).

ACKNOWLEDGEMENTS

The authors are very grateful to the Competence Center in Energy and Mobility CCEM, Swisselectric Research and the foundation The Ark through the program The Ark Energy for their financial support

REFERENCES AND CITATIONS

[1] Roussopoulos, K & Monkewitz, P. A (2000). Measurements of Tip Vortex Characteristics and the Effect of an Anti-Cavitation Lip on a Model Kaplan Turbine Blade, *Flow, Turbul. Combust*., **64**, 119–144.

[2] Kang, S & Hirsch, C (1993). Experimental study on three dimensional flow within a compressor cascade with tip clearance: part II: the tip leakage vortex. *ASME J. Turbomach*, **115**, 444–452.

[3] Muthanna, C & Devenport, W. J (2004). Wake of a Compressor Cascade with Tip Gap , Part 1 : Mean Flow and Turbulence Structure, *AIAA J.*, **42**, no 11, 2320–2331.

[4] Wang, Y & Devenport, W. J.(2004). Wake of a Compressor Cascade with Tip Gap , Part 2 : Effects of Endwall Motion*, AIAA J.*, **42**, no 11, 2332–2340.

[5] Devenport, W. J. & Rife, M. C. (1996). The structure and development of a wing-tip vortex, *J. Fluid Mech.*, **312**, 67–106.

[6] Higashi, S, Yoshida, Y. & Tsujimoto, Y. (2002).Tip Leakage Vortex Cavitation from the Tip Clearance of a Single Hydrofoil, *JSME Int. J.*, **45**, no. 3.

[7] Kunz, R.F. & Lakshminarayana, B. (1992). Three-dimensional Navier Stokes computation of turbomachinery flows using an explicit numerical procedure and a coupled k-ε turbulence model. *ASME J. Turbomach*, **114**, 627–642.

[8] Borello, D & Hanjalic, K. (2007). Computation of tip-leakage flow in a linear compressor cascade with a second-moment turbulence closure, *Int. J. Heat Fluid Flow*, **28**, 587–601.

[9] You, D., Wang, M., Moin, P. & Mittal, R. (2007). Large-eddy simulation analysis of mechanisms for viscous losses in a turbomachinery tip-clearance flow, *J. Fluid Mech.*, **586**, 177–204.

[10] You, D., Wang, M., Moin, P. & Mittal, R. (2006). Effects of tip-gap size on the tip-leakage flow in a turbomachinery cascade, *Phys. Fluids*, **18**, no. 10.

[11] Watanabe, S., Seki, H., Higashi, S., Yokota, K. & Tsujimoto, Y.(2001). Modeling of 2-D Leakage Jet Cavitation as a Basic Study of Tip Leakage Vortex Cavitation, *J. Fluids Eng.*, **123**, 50–56.

[12] Miorini, R. L. & Katz, J. (2012). The Internal Structure of the Tip Leakage Vortex Within the Rotor of an Axial Waterjet Pump, *J. Turbomach.*, **134**.

[13] Ugajin, K. & Matsumoto, H. (2009). Numerical Analysis of the Inlfuence of the Tip Clearence Flows on the unsteady cavitating flows in a three-dimensional Inducer, *J. Hydrodyn.*, **21**, no. 1, 34–40.

[14] Cupillard, S (2013). CFD Simulation of the Tip Vortex Cavitation in a Propeller Turbine. 5th International Workshop on Cavitation and Dynamic Problems in Hydraulic Machinery, Lausanne, Switzerland.

[15] Numerical Computations of a Tip Vortex Including Gap with RANS and LES Turbulence Models. 5th International Workshop on Cavitation and Dynamic Problems in Hydraulic Machinery, Lausanne, Switzerland.

[16] Dreyer, M. & Farhat, M. (2013). Experimental Characteristics of Tip Leakage Vortex Dynamics. 5th International Workshop on Cavitation and Dynamic Problems in Hydraulic Machinery, Lausanne, Switzerland.

[17] Menter, F. R. (2009). Review of the shear-stress transport turbulence model experience from an industrial perspective, *Int. J. Comput. Fluid Dyn.*, **23**, no. 4, 305–316.

[18] Kunz, R. F., Boger, D. A., Stinebring, D. R., Chyczewski, S., Lindau, J. W., Gibeling, H. J., Venkateswaran, S. & Govindan, T. R. (2000). A preconditioned Navier - Stokes method for two-phase Flows with application to cavitation prediction, *Comput. Fluids*, **29**, 849–875.